



# Numerical Simulation of the Non-Isothermal Co-Extrusion Fiber Spinning with Flow-Induced Crystallization

B. E. García<sup>1†</sup>, A. Zacarías<sup>2</sup>, V. H. Ferrer<sup>3</sup> and R. O. Vargas<sup>2</sup>

<sup>1</sup> *Facultad de Estudios Superiores Zaragoza, UNAM, Batallón del 5 de Mayo s/n, esquina Fuerte de Loreto, Col. Ejército de Oriente, Delegación Iztapalapa, C. P., 09320, Ciudad de México, Mexico*

<sup>2</sup> *ESIME Azcapotzalco, Instituto Politécnico Nacional, Avenida de las Granjas No. 682, Colonia Santa Catarina, Delegación Azcapotzalco, Ciudad de México, 02250 Mexico*

<sup>3</sup> *ESIME Zacatenco, Instituto Politécnico Nacional, U.P. Adolfo López Mateos, Col. Lindavista, Del. Gustavo A. Madero, Ciudad de México, 07738, Mexico*

† *Corresponding Author Email: iqblanca@comunidad.unam.mx*

(Received August 16, 2017; accepted February 3, 2018)

## ABSTRACT

In this work, the numerical simulation of the non-isothermal steady co-extrusion fiber spinning with flow-induced crystallization is explored. The model is based on the formulation originally proposed by China *et al.* in which Newtonian and Phan-Thien-Tanner (PTT) fluids are considered the core and the skin layer, respectively. The polymeric flow rate fraction, Deborah dimensionless number and the PTTs parameters on the temperature, the velocity and the crystallization profiles are analyzed. The numerical results show: the temperature profile is sensitive to the polymeric layer flow rate and the deformation parameters (shear thinning and extensional), the tensile stress induced crystallization parameter has a strong influence at the onset of the process, increasing drastically temperature and crystallinity.

**Keywords:** Polymer processing; PTT model; FIC.

## NOMENCLATURE

$A$	cross sectional area	$T_{max}$	maximum crystallization temperature
$A_0$	transversal section area at $z = 0$	$T_a$	environment temperature
$\sigma$	stress tensor	$T_0$	temperature at $z = 0$ of the fiber
$\sigma_{rr}$	stress in the radial direction	$F$	draw force applied at $z = L$
$\sigma_{zz}$	stress in the axial direction	$\kappa$	flow-induced crystallization factor
$\phi$	the flow rate fraction of the skin-layer	$n$	avrami index
$\xi$	shear thinning/thickening PTT parameter	$a$	dimensionless area
$\varepsilon$	the extensional PTT parameter	$v$	dimensionless velocity
$z$	axial direction	$\tau_{ii}$	dimensionless stress
$D$	strain tensor	$\chi$	dimensionless crystallinity parameter
$\mu^c$	core layer viscosity	$\theta$	dimensionless temperature
$\mu^s$	skin layer viscosity	$\zeta$	dimensionless axial position
$V_0$	initial velocity	$M$	viscosity ratio
$V_L$	final velocity	$N$	dimensionless first normal stress difference
$E$	elastic modulus	$G$	dimensionless axial force
$\lambda$	relaxation time	$St$	Stanton number
$L$	velocity gradient	$De$	Deborah number
$tr \sigma^s$	trace of stress tensor	$Dr$	draw ratio
$\Delta H_f$	heat of crystallization per unit mass	$\Delta H_f^*$	dimensionless crystallization heat
$C_p$	heat capacity of the skin fluid	$\frac{\Delta H_f X_\infty}{C_p T_0}$	
$X$	the crystallinity	$w$	dimensionless axial strain
$\rho$	skin fluid density		
$X_\infty$	maximum crystallinity		

## 1. INTRODUCTION

Many economic and technical advantages have been found in co-extrusion, it has gained wide recognition a polymer processing technique capable of achieving unique product performance, by combining the properties of different materials at lower cost [Hufenus \*et al.\* \(2012\)](#), [Perret \*et al.\* \(2013\)](#), [Reifler \*et al.\* \(2014\)](#). Modeling and simulation of co-extrusion process require simultaneous consideration of constitutive and mass, momentum and energy conservation equations. The complete understanding of the process needs to take into account important features reported in the literature like discontinuities at the interface, non-Newtonian behavior, encapsulation phenomena and the implementation of numerical techniques ([Liu and Beris 1988](#)).

The fiber spinning theory has been studied by many research groups [Kase and Matsuo \(1965\)](#), [Sung \*et al.\* \(2005\)](#), [Denn \*et al.\* \(1975\)](#), [Ziabicki \(1976\)](#), [Joo \*et al.\* \(2002\)](#). Important aspects of stability and instability phenomenon observed in the spinning process have attracted researchers attention for both academic and industry [Pearson and Matovich \(1978\)](#), [White and Ide \(1978\)](#), [Fisher and Denn \(1976\)](#), [Gelder \(1971\)](#), [Beris and Liu \(1988\)](#). The transient solution of the fiber spinning with and without flow-induced crystallization (FIC) is indispensable to developing strategies for stabilization and optimization [Lee and Park \(1995\)](#). The FIC involves complex cinematics and thermal conditions, the phase transition is extremely sensitive to flow deformation and the material exhibits a non-Newtonian behavior. Consequently, a good understanding of FIC dynamics is crucial in high-speed melt spinning modeling. Complete reviews of FIC can be found in [McHugh \(1990\)](#), [Eder \*et al.\* \(1990\)](#), [Sung \*et al.\* \(2005\)](#).

In regard of the interaction of two fluids, [Lee and Park \(1995\)](#) studied the draw resonance instability using a model where Newtonian and Upper-Convected Maxwell fluids (UCM) as the core and the skin layer, respectively. For an isothermal spinning flow, [Ching-China and Jyh-Chau \(1996\)](#) analyzed the influence of flow-rate ratio, Deborah number and deformation parameters (extensional and shear) on the spinline velocity. In their model Newtonian and PTT fluids were considered the core and the skin layer, respectively. For the non-isothermal co-extrusion flow, [Nordberg and Winter \(1990\)](#) used the Warner model like the skin layer. They reported that it is possible to predict the stability of the process through the viscosity ratio at the interface and the normal stress difference ratio.

In the present work, the non-isothermal co-extrusion fiber spinning with flow-induced crystallization is analyzed. The present model and the numerical simulation is an extension of the formulation originally proposed by [Ching-China and Jyh-Chau \(1996\)](#) in which Newtonian and PTT fluids are considered the core and the skin

layer, respectively. The crystallization is taken into account using the kinetic equation used by [Sung \*et al.\* \(2005\)](#). The analysis is limited to the draw down region, where the fluids are stretched to form a thin fiber; the inertia, gravitational and surface tension are neglected. The influence of the polymeric flow rate fraction, the PTTs parameters model, the Deborah number and the flow induced crystallization is analyzed.

## 2. MATHEMATICAL MODEL

### 2.1 Assumptions

A simplified scheme of the co-extrusion fiber process is shown in Fig. 1. According to material properties and process conditions such as; incompressible and viscous fluid, low Reynolds number (ratio of inertial forces to viscous forces) and low weight material. The main assumptions of the model are: i) steady-state and non-isothermal flow, ii) the core and skin layer are Newtonian and PTT fluids, respectively, iii) crystallization kinetics for the skin layer is considered, iv) viscous and viscoelastic force are included and v) gravity, inertia and surface tension are neglected.

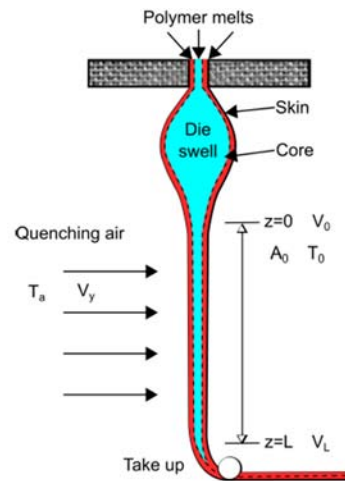


**Fig. 1. Schematic diagram of the co-extrusion spinning process.**

### 2.2 Governing Equations

According to the above assumptions, the mass and momentum equations are:

$$\frac{\partial(AV_z)}{\partial z} = 0, \quad (1)$$

$$\frac{\partial}{\partial z} \left[ \phi A (\sigma_{zz}^s - \sigma_{rr}^s) + (1 - \phi) (\sigma_{zz}^c - \sigma_{rr}^c) \right] = 0. \quad (2)$$

The first term in Eq. (2) is the axial tension contributed by PTT skin fluid while the second term is caused by the Newtonian core layer.

### 2.3 Constitutive Equations

For the Newtonian core layer, the stress tensor  $\sigma^c$  is proportional to the strain rate  $\mathbf{D}$  as follows:

$$\sigma^c = -2\mu D \quad (3)$$

The radial and axial stress tensor components are, respectively

$$\sigma_{rr}^c = -\mu^c \frac{\partial V_r}{\partial r}, \quad \sigma_{zz}^c = -2\mu^c \frac{\partial V_z}{\partial z}. \quad (4)$$

The PTT constitutive equation, known for its robustness and accuracy in describing extensional deformation processes, is employed for the skin layer. The exponential PTT model is:

$$\exp\left(\frac{\varepsilon}{E} \text{tr} \sigma^s\right) \sigma^s + \lambda \left( (V \cdot \nabla) \sigma^s - L \cdot \sigma^s - \sigma^s \cdot L \right) = 2\mu^s D, \quad (5)$$

$$\text{tr} \sigma^s = \sigma_{rr} + \sigma_{\theta\theta} + \sigma_{zz} = 2\sigma_{rr} + \sigma_{zz}, \quad (6)$$

$$L = \nabla V - \xi D, \quad (7)$$

where  $E$ ,  $\text{tr} \sigma^s$ ,  $\lambda$  and  $L$  are the elastic modulus, the trace of stress tensor, the relaxation time and the velocity gradient tensor, respectively. The dimension-less parameters  $\varepsilon$  and  $\xi$  represent the extensional and the shear thinning/thickening effects, respectively.

In the case of steady state uniaxial flow, Eq. (5) for radial and axial stresses is [Ching-China and Jyh-Chau \(1996\)](#):

$$\sigma_{rr} \exp\left(\frac{\varepsilon \lambda}{\mu^s} (\sigma_{zz} + 2\sigma_{rr})\right) + \lambda (V_z \frac{\partial \sigma_{rr}}{\partial z} + (1 - \xi) \frac{\partial V_z}{\partial z} \sigma_{rr}) = -\mu^s \frac{\partial V_z}{\partial z}. \quad (8)$$

$$\sigma_{zz} \exp\left(\frac{\varepsilon \lambda}{\mu^s} (\sigma_{zz} + 2\sigma_{rr})\right) + \lambda (V_z \frac{\partial \sigma_{zz}}{\partial z} - 2(1 - \xi) \frac{\partial V_z}{\partial z} \sigma_{zz}) = 2\mu^s \frac{\partial V_z}{\partial z}. \quad (9)$$

## 2.4 Energy Equation

Considering absence of resistance to radial heat transfer by conduction between layers and in the axial direction but accounting the heat exchange between skin layer and surrounding and the crystallization kinetic the energy equation is:

$$V_z \frac{\partial T}{\partial z} = -\frac{2\sqrt{\pi} h}{\rho C_p \sqrt{A}} (T - T_a) + \frac{\Delta H_f}{C_p} (V_z \frac{\partial X}{\partial z}), \quad (10)$$

where  $\Delta H_f$ ,  $h$ ,  $T_a$ ,  $X$ ,  $C_p$  and  $\rho$  are the heat of crystallization per unit mass, the heat transfer coefficient, the environment temperature, the crystallinity, the heat capacity and the density of skin fluid, respectively.

## 2.5 Crystallization Equation

For the crystallization kinetics, the model used by [Joo \*et al.\* \(2002\)](#) and [Sung \*et al.\* \(2005\)](#) is implemented here. In this model the crystallization rate is a function of temperature and of the molecular orientation. Then, in uniaxial extensional flow this molecular

orientation is related to the first normal stress difference as.

$$V_z \frac{\partial X}{\partial z} = n \left( \ln \left( \frac{X_\infty}{X_\infty - X} \right) \right)^{\frac{n-1}{n}} (X_\infty - X) K_{max} \exp\left(-4 \ln 2 \left( \frac{T - T_{max}}{D} \right)^2 + \kappa \left( \frac{\sigma_{zz} - \sigma_{rr}}{E} \right)\right), \quad (11)$$

where  $X$  and  $X_\infty$  are the crystallinity and the maximum crystallinity, respectively.  $T_{max}$  is the fluid temperature at the maximum crystallization rate,  $K_{max}$  is the maximum crystallization rate,  $\kappa$  is the flow-induced crystallization factor and  $n$  is the Avrami index that in the case of uniaxial extension is one.

The set of Eqs. (1, 2, 8, 9, 10 and 11) is placed in dimensionless form using the following scaling parameters  $a$ ,  $v$ ,  $\tau_{ii}$ ,  $x$ ,  $\theta$ ,  $\theta_a$ ,  $v_y$ ,  $k_m$ ,  $d$  and  $\zeta$  defined as:

$$a = \frac{A}{A_0}, \quad v = \frac{V_z}{V_0}, \quad \tau_{ii} = \frac{\sigma_{ii} A_0}{F}, \quad \chi = \frac{X}{X_\infty}, \quad \theta = \frac{T}{T_0}, \\ \theta_a = \frac{T_a}{T_0}, \quad \theta_{max} = \frac{T_{max}}{T_0}, \quad k_m = \frac{k_{max} L}{V_0}, \quad d = \frac{D}{T_0}, \quad \zeta = \frac{z}{L}.$$

## 2.6 Dimensionless Equations

$$\frac{d v}{d \zeta} = 0, \quad (12)$$

$$\frac{d}{d \zeta} \left[ a \phi N + 3(1 - \phi) a G M \frac{d v}{d \zeta} \right] = 0 \quad (13)$$

$$\tau_{zz} \exp\left\{ \frac{\varepsilon D e}{G} (3\tau_{zz} - 2N) \right\} + D e \left\{ v \frac{d \tau_{zz}}{d \zeta} - 2(1 - \xi) \tau_{zz} \frac{d v}{d \zeta} \right\} = 2G \frac{d v}{d \zeta}, \quad (14)$$

$$N \exp\left\{ \frac{\varepsilon D e}{G} (3\tau_{zz} - 2N) \right\} + D e \left\{ v \frac{d N}{d \zeta} + (1 - \xi) N \frac{d v}{d \zeta} - 3(1 - \xi) \tau_{zz} \frac{d v}{d \zeta} \right\} = 3G \frac{d v}{d \zeta} \quad (15)$$

$$v \frac{d \theta}{d \zeta} = -S_t a^2 (\theta - \theta_a) + \Delta H_f^* (v \frac{d x}{d \zeta}), \quad (16)$$

$$v \frac{d x}{d \zeta} = (1 - x) k_m \exp\left[ -4 \ln 2 \left( \frac{\theta - \theta_{max}}{d} \right)^2 + \frac{\kappa N D e}{G} \right], \quad (17)$$

Where

$$\Delta H_f^* = \Delta H_f X_\infty / C_p T_0, \quad N = \tau_{zz}^s - \tau_{rr}^s, \quad M =$$

$\mu^c / 2\mu_0^s$  and  $G = \mu^s A_0 V_0 / FL$  are; the dimension-less crystallization heat, the first normal stress difference, the ratio of the core and skin viscosity in the fiber and the dimensionless axial force, respectively. Finally

$S_t = 3.55 h L / \rho C_p V_0 A_0^{1/2}$  is Stanton number and

$De = \lambda V_0 / L$  is Debora number.

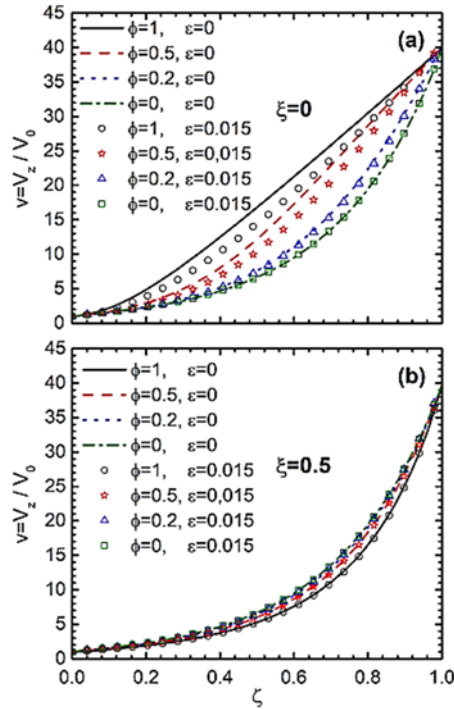


**Fig. 2. Velocity profile as a function of dimensionless position for (a) extensional and (b) extensional+ shear deformations.**

### 2.7 Boundary Conditions

The dimensionless boundary conditions for velocity, cross area, first normal stress difference, axial stress, temperature and crystallinity at the beginning and at the end of the fiber are:

$$\text{at } \zeta = 0; \quad a = 1, v = 1, N = 1, \tau_{zz} = t_0, \theta = 1, x_c = 0 \quad (18)$$

$$\text{at } \zeta = 1; \quad v = D_r = \frac{V_L}{V_0},$$

where  $D_r$  is the draw ratio indicating the relation between

the take up velocity  $V_L$  and the velocity at the beginning of the fiber  $V_0$ .  $D_r$  determines the final condition for all the others variables, with this procedure reduce the order and grade of the differential equation for the velocity and the Eqs. (12-13) are integrated:

$$av = 1, \quad (19)$$

$$N = \frac{v}{\phi} - \frac{3(1-\phi)}{\phi} GM \frac{dv}{d\zeta}, \quad (20)$$

The value of integration constants Eqs. (19-20) are set to unity (there is no loss of generality in the solution) Ching-China and Jyh-Chau (1996). Substitution of Eqs. (19-20) into Eqs. (14) and (17) is made. A set of simultaneous first-order ordinary differential equations is obtained; this set is solved by numerical procedures Shoichiro (2001):

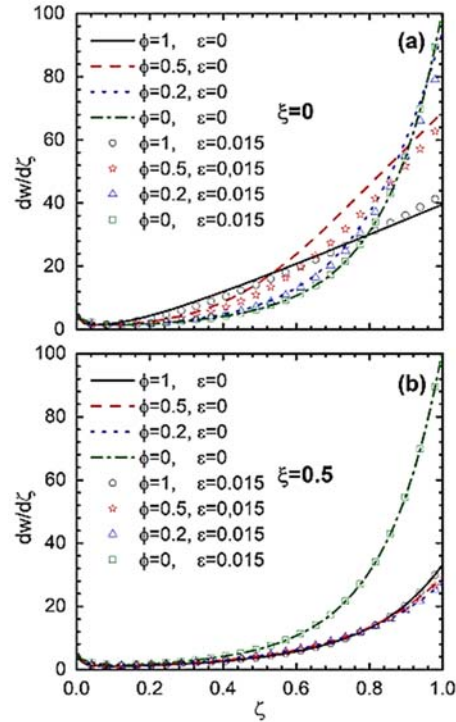


**Fig. 3. Extensional rate profile as a function of dimensionless position for (a) extensional and (b) extensional + shear deformations**

$$\frac{dv}{d\zeta} = w, \quad (21)$$

$$\frac{dw}{d\zeta} = \frac{\exp(B)}{3(1-\phi)MGDe} - \frac{w}{v} \left[ \frac{\exp(B)}{De} + (1-\xi)w \right] - \frac{w}{(1-\phi)M} \left[ \frac{\phi}{2vDe} - \left( \frac{2-\xi}{3G} \right) + \left( \frac{\phi(1-\xi)\tau_{zz}}{vG} \right) \right] \quad (22)$$

$$\frac{d\tau_{zz}}{d\zeta} = [2G + 2De(1-\xi)\tau_{zz}] \frac{w}{vDe} - \frac{\tau_{zz}\exp(B)}{vDe}, \quad (23)$$

$$\frac{d\theta}{d\zeta} = -S_i v^{\frac{-1}{2}} (\theta - \theta_a) + \Delta H_f^* \left( \frac{d\chi}{d\zeta} \right), \quad (24)$$

$$\frac{d\chi}{d\zeta} \quad (25)$$

$$= \frac{(1-\chi)}{v} k_m \exp \left[ -4 \ln^2 \left( \frac{\theta - \theta_{\max}}{d} \right)^2 + \frac{\left( \frac{v}{\phi} - \frac{3(1-\phi)vMG}{\phi} \right) \kappa De}{G} \right]$$

Where  $B = \frac{De}{G} \left[ 3\tau_{zz} - \frac{2v}{\phi} + \frac{6(1-\phi)6Mw}{\phi} \right]$  and

the corresponding boundary condition for Eq.  $w = \frac{1}{3MG}$  at  $\zeta = 0$  Ching-China and Jyh-Chau (1996).

### 3. RESULTS AND DISCUSSIONS

In this section, the numerical predictions of the non-isothermal co-extrusion fiber spinning with

flow-induced crystallization are presented. The influence of the PTT's parameters model ( $\epsilon, \xi = 0$ ), the polymeric flow rate fraction and the flow induced crystallization on the main variables are analyzed.

### 3.1 Solution Method

The set of Eqs. (21)-(25) along with the corresponding boundary conditions (Eq. 18) are solved numerically using the shooting method [Shoichiro \(2001\)](#).

### 3.2 Velocity Profile

Figure 2 shows the effect of the polymeric flow rate fraction on the velocity profile. In Fig. 2a, when ( $\epsilon = 0, \xi = 0$ ) the Upper Convected Maxwell (UCM) is recovered, notice that increasing  $\phi$  makes the velocity profile becomes linear, this behavior is associated with the material elasticity. The upper and lower limits ( $\phi = 1$  and  $\phi = 0$ ) correspond to elastic and viscous contributions of the material, respectively [Denn \(2008\)](#), [Bird \*et al.\* \(1987\)](#).

Similar numerical results were reported by [Ching-China and Jyh-Chau \(1996\)](#) using the UCM for the mixture PET/PP. The case of extensional deformation ( $\epsilon = 0.015, \xi = 0$ ) and varying  $\phi$ , the same behavior is obtained but in lower magnitude except for a viscous fluid  $\phi = 0$ . The Fig. 2b show the cases of shear ( $\epsilon = 0, \xi = 0.5$ ) and extensional/shear deformations ( $\epsilon = 0.015, \xi = 0.5$ ), all the velocity curves are closer and similar of the results reported by [Ching-China and Jyh-Chau \(1996\)](#) for the polymeric isothermal co-extrusion, the shear thinning effect is dominant in the PTT model and instability phenomena could happen for higher extensional rates.

### 3.3 Extensional Rate Profile

In Fig. 3 shows the extensional rate as a function of the axial position for different values of polymeric flow rate fraction, Fig. 3a shows that lower extensional rate is the UCM with  $\phi = 1$  and higher extensions for ( $\epsilon = 0.015, \xi = 0$ ) reducing  $\phi$ . At the beginning of the fiber there is a reduction of the extensional rate, which can be explained as a yield stress or the required energy for the material starts to flow, after this point a linear behavior for an elastic material with small extension and higher deformations at the end of the fiber for an extensional viscous fluid are exhibit. Considering both deformations extensional/shear ( $\epsilon = 0.015, \xi = 0.5$ ) the result is a single curve with separation at the end of the fiber Fig. 3b.

The effect of the elastic force reduces the velocity because the material tends to recover its original form and part of the total energy of the system is used in this process, the viscous case all the energy is employed in diffusional process.

### 3.4 Axial Stress Tensor

In Fig. 4 the axial stress tensor  $T_{zz}$  as a function of the position is presented, for the UCM with  $\phi = 1$ ,  $T_{zz}$  increases up to reach a constant value at the beginning of the process, it is known that UCM reports an unreal behavior for large deformations. The polymeric flow rate fraction has strong influence in this process Fig. 4a, [Takeshi \*et al.\* \(1996\)](#) used the UCM with  $\phi = 0.5$  for the ratio 5/5 PET/PP system, They reported the same behavior of this work. A significant increase of  $T_{zz}$  can be obtained incorporating the extensional parameter in the PTT model, if shear deformation is also included, the later dominates the process and modifies the behavior to a single curve reaching higher tensile stresses, see Fig. 4b.

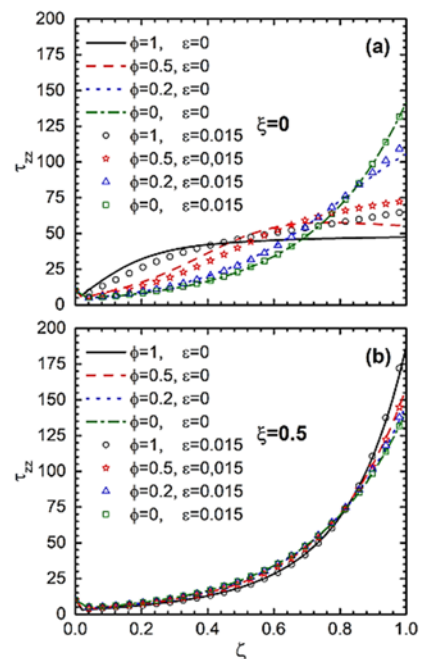


**Fig. 4. Axial stress as a function of dimensionless position for (a) extensional and (b) extensional + shear deformations**

High-speed non-isothermal melt spinning is associated with a concentrated neck-like deformation process and the development of high tensile stresses that result in the so-called flow (or axial stress) induced crystallization (FIC). In Fig. 5 shows the crystallization percentage as a function of the axial position varying the polymeric flow rate fraction  $\phi$  and the crystallinity parameter control  $\kappa$ . For  $\kappa = 0$ , no induced crystallization is considered, however the crystallinity increases up to reach a constant value Fig. 5a. [Doufas \*et al.\* \(2000\)](#) published similar results for a Nylon-66 fiber, They reported that the crystallinity is dependent on the polymeric flow rate. Extensional deformation augmented the crystallinity percentage keeping the same behavior Figs. 5a-5c.

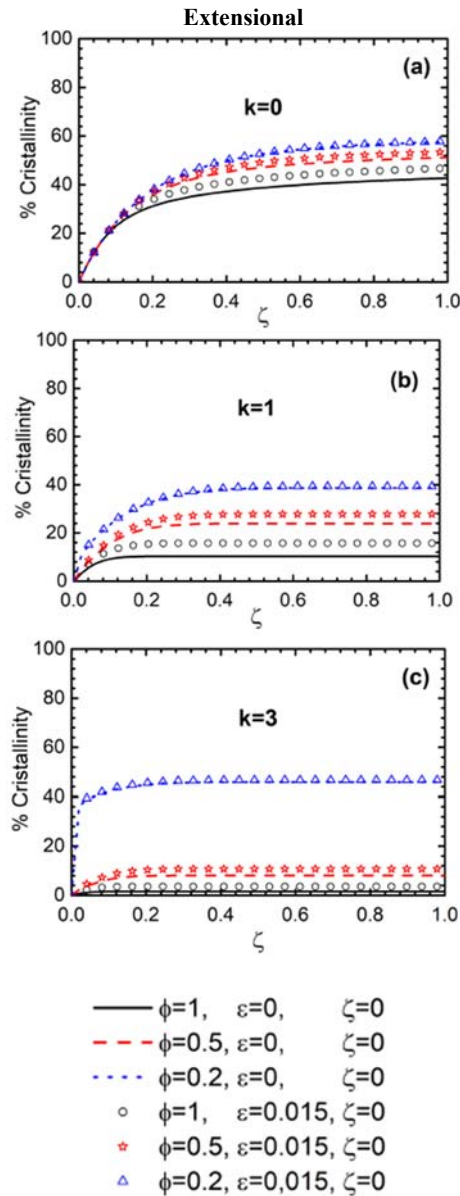


**Fig. 5. Crystallization profile as a function of dimensionless position for extensional deformation**

Increasing  $\kappa$  the crystallization process is faster but its percentage is reduced, except for a viscous fluid where the crystallinity percentage is augmented Figs. 5a-5c. In Fig. 6 the crystallinity profile for a extensional/shear deformation is shown, the crystallinity percentage increases but the shear thinning effect dominates the process due to all the curves are closer varying the polymeric flow rate fraction  $\kappa$  except for a viscous fluid where is sensible to this process.

### 3.6 Temperature Profile

The temperature profile as a function of the axial position without crystallization is shown in Fig. 7. The temperature decreases monotonically along the fiber due to the heat transfer by convection mechanism, this effect is considered in the model by the Stanton dimensionless number.

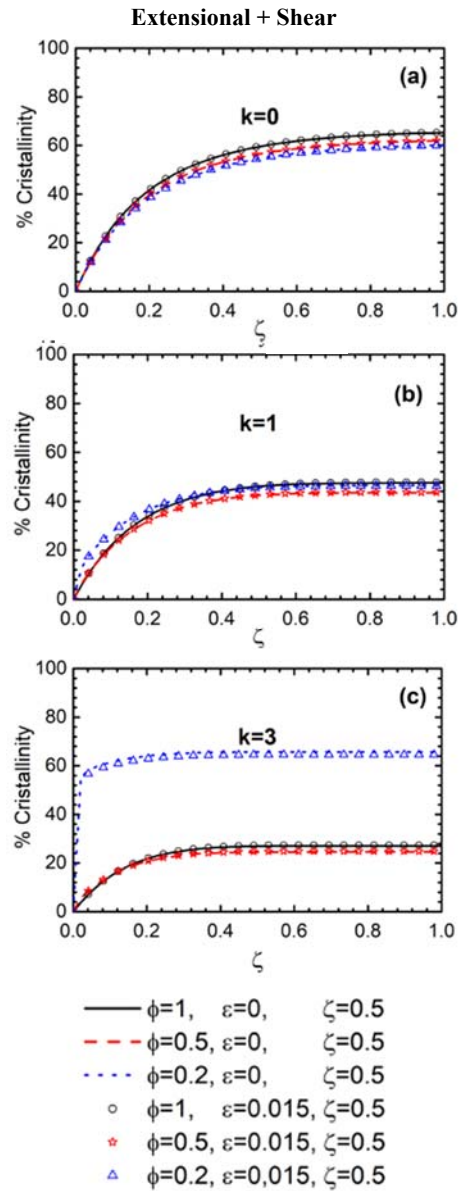


**Fig. 6. Crystallization profile as a function of dimensionless position for extensional/shear deformation**

In Figs. 7a and 7b all curves have the same behavior, the temperature along the fiber is dependent on the type of deformation and on the polymeric flow rate fraction. Takeshi *et al.* (1996) using a non-isothermal model reported similar results. Including the shear thinning effect, the temperature decrease monotonically having the same behavior of the previous one, but the curves are closer indicating the strong influence of the shear parameter  $\zeta = 0.5$  and more viscous dissipation is generated Fig. 7b.

The temperature profile taking into account the crystallinity kinetic process is shown in Fig. 8. In this figure exhibits an increment of the temperature due to crystallization effect, this behavior is reported in the numerical predictions of polymeric fiber extrusion by Eder *et al.* (1990), McHugh (1990). A strong influence of

the stress induce crys-tallization on the temperature profile is at the be-ginning of the process, see Figs 8a and 8b. The higher increment of the temperature is reached when the process takes into account a shear thinning fluid and the stress induced crystallization Fig. 9. After this process the temperature decreases monotonically due to the convection heat transfer to the environment

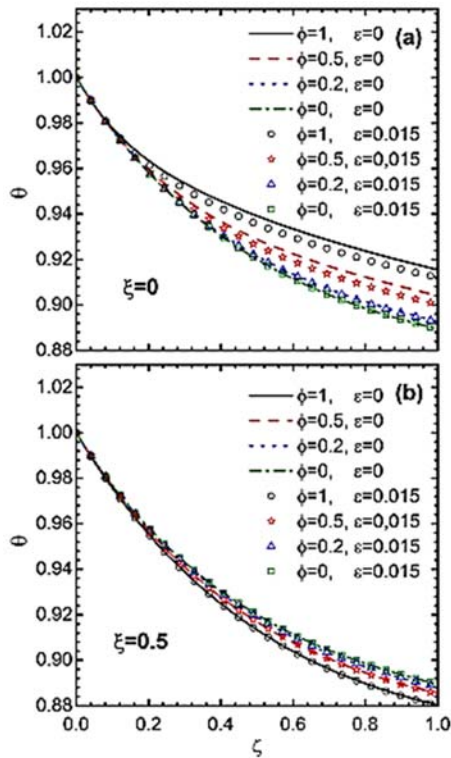


**Fig. 7. Temperature profile as a function of dimensionless position for (a) extensional and (b) extensional + shear deformations**

#### 4. CONCLUSIONS

The numerical simulation of the non-isothermal steady co-extrusion fiber spinning with flow-induced crystallization is performed. The formulation originally proposed by China *et al.* is extended, Newtonian and PTT fluids are considered the core and the skin layer, respectively.

The numerical results of the non-isothermal fiber spinning process without crystallization but taking into account the extensional and shear thinning/thickening deformation, exhibit the same behavior of the isothermal case reported by Ching-China and Jyh-Chau (1996). The extension rate, tensile stress tensor and temperature profiles are in-fluenced by the polymeric flow rate fraction and thinning parameters of the PTT model.

Higher axial stress tensor are reached when the shear thinning parameter is included in the PTT model, the shear thinning effect dominates the process, obtaining a single curve.

The extensional rate as a function of the position shows a linear behavior for high elastic fluid, this behavior is lost when viscous contribution is increased.

The extensional rate, stress tensor and temperature profiles are affected when the flow-induced crystallinity. The degree of crystallinity profile show a monotonic increased up to reach a constant value. On the other hand, the tensile stress has a strong influence on the degree of crystallinity at the be-ginning of the fiber extruded, the zone where the crystallinity is constant depend on the viscoelastic flow fraction.

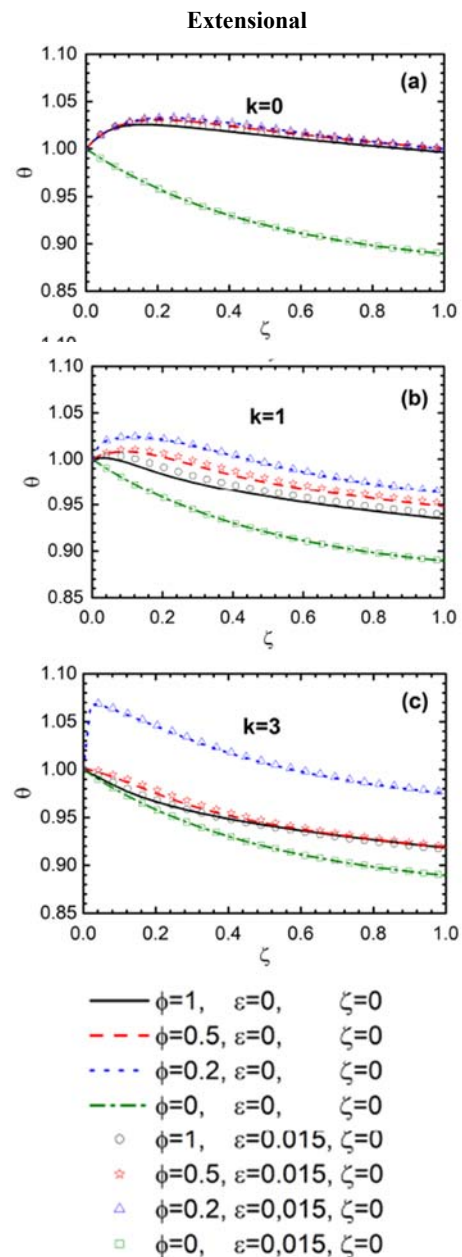


**Fig. 8. Crystallization profile as a function of dimensionless position for extensional deformation varying the crystallinity parameter  $\kappa$**

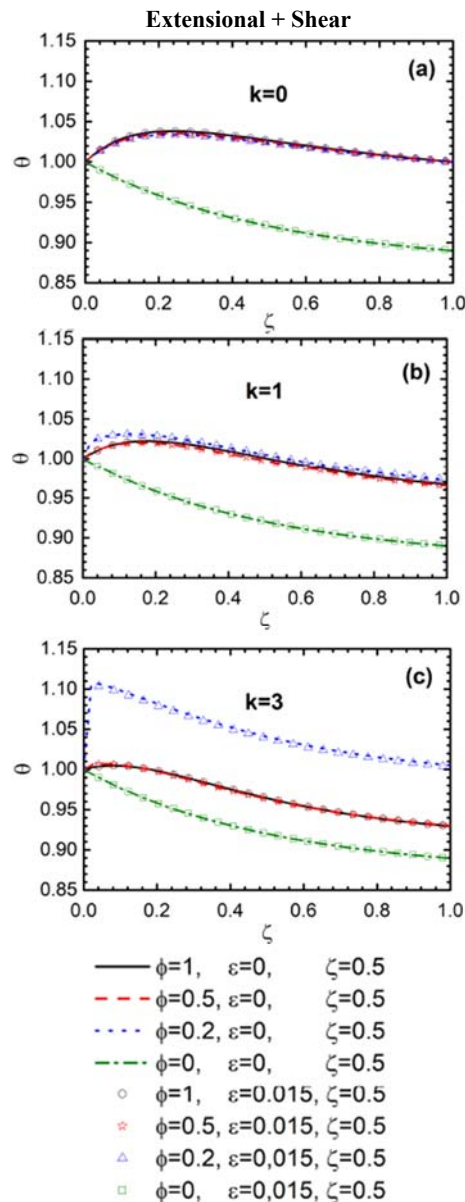


**Fig. 9. Crystallization profile as a function of dimensionless position for extensional + shear deformations varying the crystallinity parameter  $\kappa$**

### ACKNOWLEDGMENTS

First author would like to acknowledge the financial support from UNAM-PAPIIT-IA106518. R.O. Vargas gratefully acknowledges support by SIP-IPN 20171482.

### REFERENCES

Beris, A. and B. Liu (1988). Time-dependent fiber spinning equations I. analysis of the mathematical behavior. *Journal of Non-Newtonian Fluid Mechanics* 26(-), 341361.

Bird, R., R. Armstrong, and O. Hassager (1987). *Dynamics of polymeric liquids*. UK.: John Wiley.

Ching-China, J. and Y. JyhChau (1996). Mechanics of steady flow in coextrusion fiber spinning. *Polymer Engineering and Science* 36(10), 1399–1409.

Denn, M. (2008). *Polymer Melt Processing, Foundations in Fluid Mechanics and Heat Transfer*. USA: Cambridge University Press.

Denn, M., C. Petrie, and P. Avenas (1975). Mechanics of steady spinning of a viscoelastic liquid. *American Institute of Chemical Engineering* 21(-), 791799.

Doufas, A., A. McHugh, and C. Miller (2000). Simulation of melt spinning including flow-induced crystallization part i. model development and predictions. *Journal of Non-Newtonian Fluid Mechanics* 92(-), 27–66.

Eder, G., H. Janeschitz-Kriegl, and S. Liedauer(1990). Crystallization processes in quiescent and moving polymer melts under heat transfer conditions. *Prog. Polym. Sci* 15, 629–714.

Fisher, R. and M. Denn (1976). A theory of isothermal melt spinning and draw resonance. *American Institute of Chemical Engineering* 22, 236246.

Gelder, D. (1971). The stability of fiber drawing processes. *Ind. Industrial & Engineering Chemistry Fundamentals* 10, 534535.

Hufenus, R., F. A. Reifler, K. Maniura-Weber, A. Spierings, and M. Zinn (2012). Biodegradable bicomponent fibers from renewable sources: Melt-spinning of poly(lactic acid) and poly[(3-hydroxybutyrate)-co-(3-hydroxyvalerate)]. *Macromolecular Materials and Engineering* 297(1), 75–84.

Joo, Y., J. Sun, M. Smith, R. Armstrong, R. Brown, and R. Ross (2002). Two-dimensional numerical analysis of non-isothermal melt spinning with and without phase transition. *Journal of Non-Newtonian Fluid Mechanics* 102, 37–70.

Kase, S. and T. Matsuo (1965). Studies on melt spinning. i. fundamental equations on the dynamics of melt spinning. *Journal of Polymer Science Part A* 3, 2541–2554.

Lee, W. and C. Park (1995). Stability of a bicomponent fiber spinning flow. *Journal of Applied Mechanics* 62, 511–516.

Liu, B. and A. Beris (1988). Time-dependent fiber spinning equations. 2. analysis of the stability of numerical approximation. *Journal of Non-Newtonian Fluid Mechanics* 26, 363394.

McHugh, A. (1990). Mechanisms of flow-induced crystallization. *Polymer Engineering and Science* 22, 15–26.

Nordberg, M. and H. Winter (1990). A simple model of nonisothermal coextrusion. *Polymer Engineering and Science* 30, 408–416.

- Pearson, J. and M. Matovich (1978). Spinning amolten thread line: stability. *Industrial & Engineering Chemistry Fundamentals* 8, 605609.
- Perret, E., F. A. Reifler, R. Hufenus, O. Bunk, and M. Heuberger (2013). Modified crystallization in pet/pps bicomponent fibers revealed by small-angle and wide-angle x ray scattering. *Macromolecules* 46, 440–448.
- Reifler, F. A., R. Hufenus, M. Krehel, E. Zraggen, R. M. Rossi, and L. J. Scherer (2014). Polymer optical fibers for textile applications e bicomponent melt spinning from cyclic olefin polymer and structural characteristics revealed by wide angle x-ray diffraction. *Polymer* 55, 5695–5707.
- Shoichiro, N. (2001). *Numerical analysis andgraphic visualization with MATLAB*. -: Person Education.
- Sung, L., S. Myeong, J. Hyun-Wook, andH. Chun (2005). Transient solutions o the dynamics in low-speed fiber spinning process accompanied by flow-induce crystal-lization. *Journal of Non-Newtonian Fluid Mechanics* 130, 110–116.
- Takeshi, K., J. Radhakrishnan, A. Sadaaki, T. Akira, O. Norimasa, J. Xia, N. Fumio, and K. Yosuke (1996). High-speed melt spinning of bicomponent fibers mechanism of fiber structure development in poly(ethylenetephtalate)/polypropylene system. *Journal of Applied Polymer Science* 62, 1913–1924.
- White, J. and Y. Ide (1978). Instabilities and failure in elongational flow and melt spinning of fibers. *Journal of Applied Polymer Science* 22, 30573074.
- Ziabicki, A. (1976). *Fundamentals of Fiber Formation*. USA: Wiley-Interscience, New York.